THE JOURNAL OF BIOLOGICAL CHEMISTRY VOL. 287, NO. 42, pp. 35589–35598, October 12, 2012

Probing the Structural Basis of Zn^{2+} Regulation of the Epithelial Na^+ Channel*

Received for publication, June 22, 2012, and in revised form, August 14, 2012 Published, JBC Papers in Press, August 28, 2012, DOI 10.1074/jbc.M112.394734

Jingxin Chen‡, Katie L. Winarski‡, Mike M. Myerburg‡, Bruce R. Pitt§, and Shaohu Sheng‡1

From the ‡Department of Medicine, School of Medicine, and §Department of Environmental and Occupational Health, Graduate School of Public Health, University of Pittsburgh, Pittsburgh, Pennsylvania 15261

Background: Extracellular Zn^{2+} regulates epithelial Na^+ channel (ENaC) activity.
Results: Specific mutations selectively weaken either the stimulatory or inhibitory effect of Zn^{2+}.
Conclusion: External Zn^{2+} regulates ENaC by interacting with multiple extracellular sites within the γ-subunit.
Significance: This report provides novel insights into the structural basis of Zn^{2+} regulation of ENaC.

Extracellular Zn^{2+} activates the epithelial Na^+ channel (ENaC) by relieving Na^+ self-inhibition. However, a biphasic Zn^{2+} dose response was observed, suggesting that Zn^{2+} has dual effects on the channel (*i.e.* activating and inhibitory). To investigate the structural basis for this biphasic effect of Zn^{2+}, we examined the effects of mutating the 10 extracellular His residues of mouse γENaC. Four mutations within the finger subdomain (γH193A, γH200A, γH202A, and γH239A) significantly reduced the maximal Zn^{2+} activation of the channel. Whereas γH193A, γH200A, and γH202A reduced the apparent affinity of the Zn^{2+} activating site, γH239A diminished Na^+ self-inhibition and thus concealed the activating effects of Zn^{2+}. Mutation of a His residue within the palm subdomain (γH88A) abolished the low-affinity Zn^{2+} inhibitory effect. Based on structural homology with acid-sensing ion channel 1, γAsp^{516} was predicted to be in close proximity to γHis^{88}. Ala substitution of the residue (γD516A) blunted the inhibitory effect of Zn^{2+}. Our results suggest that external Zn^{2+} regulates ENaC activity by binding to multiple extracellular sites within the γ-subunit, including (i) a high-affinity stimulatory site within the finger subdomain involving His^{193}, His^{200}, and His^{202} and (ii) a low-affinity Zn^{2+} inhibitory site within the palm subdomain that includes His^{88} and Asp^{516}.

Sodium transport mediated by the epithelial Na^+ channel (ENaC)[2] plays an important role in the maintenance of extracellular fluid volume and regulation of blood pressure and in the regulation of airway surface liquid volume. Altered channel activity induced by mutations of ENaC genes results in several disorders, including Liddle syndrome and pseudohypoaldosteronism type 1, and contributes to the pathogenesis of cystic fibrosis (1–4). Specific ENaC variants are suggested to contribute to the genesis of essential hypertension in selected populations (5–7).

ENaC activity is regulated by a variety of extracellular factors, including proteases, shear stress, pH, anions, nucleotides, and transition metals (8–15). Although some metals are essential for normal physiological function, excessive environmental exposure can be toxic (16, 17). For instance, particulate matter and airborne particles containing high amounts of transitional metals, including zinc and copper, contribute to pulmonary and cardiovascular toxicity (18, 19). Although recent studies have suggested that ion channels are potential molecular targets of transition metals (20), the mechanisms that confer the harmful effects of heavy metals are poorly understood.

Zinc is the second most abundant transition metal in living organisms and is thought to complex with ~10% of the human proteome (21). It has catalytic, structural, or regulatory roles in proteins that are involved in diverse biological processes (22). For example, zinc regulates voltage- and ligand-gated ion channels and may function as a signaling ion in brain (23, 24). Zinc may play a pathophysiological role in several disorders such as Alzheimer disease, cancer, diabetes, and depression (22).

Previous studies have demonstrated that low concentrations of extracellular Zn^{2+} activate ENaC. Zn^{2+} increases short-circuit current in amphibian epithelia expressing native Na^+ channels (8). Zn^{2+} activates ENaCs in heterologous expression systems by directly interacting with the channel and altering channel gating (25). Single channel recordings revealed that external Zn^{2+} increased the number of observed channels within a patch without changing single channel conductance (10). The response of ENaC to extracellular Zn^{2+} is biphasic. Low concentrations of Zn^{2+} activate the channel, with a maximal response at 100 μM Zn^{2+}. Further increases in $[Zn^{2+}]$ reduce channel activity. This bell-shaped dose-response relationship suggests that Zn^{2+} enhances channel activity at low concentrations and is inhibitory at high concentrations (25). The stimulatory effect of Zn^{2+} on ENaC has been attributed to relief of Na^+ self-inhibition (25). Na^+ self-inhibition is a rapid down-regulation of ENaC open probability when the extracellular Na^+ concentration increases (9, 26). However, the Zn^{2+}-binding sites within ENaC have not been identified, and the biphasic dose response to the heavy metal has not been explained.

ENaCs are typically composed of three homologous subunits, each of which contains short intracellular N and C ter-

* This work was supported, in whole or in part, by National Institutes of Health Grants R01 ES014701, K08 HL087932, and P30 DK079307.
[1] To whom correspondence should be addressed: Renal-Electrolyte Div., University of Pittsburgh, S929 Scaife Hall, 3550 Terrace St., Pittsburgh, PA 15261. Tel.: 412-648-9295; Fax: 412-383-8956; E-mail: shaohu@pitt.edu.
[2] The abbreviations used are: ENaC, epithelial Na^+ channel; γmENaC, mouse γENaC; cASIC1, chicken acid-sensing ion channel 1; ECD, extracellular domain.

mini, two transmembrane domains, and a large extracellular region. The crystal structure of the chicken acid-sensing ion channel 1 (cASIC1; homologous to ENaC) reveals a trimeric channel complex with a large extracellular domain (ECD) connected to the transmembrane domain via a wrist region (27). The extracellular region of a subunit is organized into five subdomains, referred to as palm, β-ball, knuckle, finger, and thumb. Recent studies suggest that the extracellular regions of ENaC subunits have a similar overall design to that of cASIC1 and that the ECD may sense various extracellular signals (12, 14, 28–31). However, the exact locations where most extracellular factors interact with ENaC and the mechanistic details of how the initial contacts lead to altered channel activity remain elusive.

The ECDs of ENaC subunits contain numerous residues, such as His, Cys, Glu, and Asp, which are capable of serving as Zn^{2+}-binding ligands (32). We hypothesized that some of these residues mediate Zn^{2+} interaction with ENaC. Several lines of evidence suggest that the γ-subunit has a particularly important role in regulating channel gating in response to external factors (11, 33, 34). Mutations were introduced into His residues within the γ-subunit ECD to identify sites that have a role in the regulation of ENaC by Zn^{2+}. Three His residues were identified within the finger subdomain that participate in a high-affinity Zn^{2+} activating site. Additionally, mutation of a palm subdomain His residue altered the low-affinity inhibitory response. These His residues are unique to the γ-subunit, as they are not found at the homologous sites in the α- and β-subunits.

EXPERIMENTAL PROCEDURES

Site-directed Mutagenesis—Point or multiple mutations were generated in mouse γENaC (γmENaC) cDNA in the pBluescript SK^- vector (Stratagene, La Jolla, CA) using the QuikChange II XL site-directed mutagenesis kit (Stratagene). Following mutagenesis, cDNAs were validated by sequencing. Wild-type ENaC α-, β-, and γ-subunit and mutant ENaC γ-subunit cRNAs were made using T3 RNA polymerase (Ambion), purified using an RNA purification kit (Qiagen), and quantified by spectrophotometry.

ENaC Expression and Two-electrode Voltage Clamp—ENaC expression in *Xenopus* oocytes and two-electrode voltage clamp were performed as reported previously (35). Stage V and VI oocytes free of follicle cell layers were injected with 1 ng of cRNA for each mENaC subunit per oocyte and incubated at 18 °C in modified Barth's saline (88 mM NaCl, 1 mM KCl, 2.4 mM $NaHCO_3$, 15 mM HEPES, 0.3 mM $Ca(NO_3)_2$, 0.41 mM $CaCl_2$, 0.82 mM $MgSO_4$, 10 μg/ml sodium penicillin, 10 μg/ml streptomycin sulfate, and 100 μg/ml gentamycin sulfate, pH 7.4).

All experiments were carried out at room temperature (20–24 °C). Two-electrode voltage clamp was performed using either an Axoclamp 900A amplifier (Molecular Devices, Sunnyvale, CA) or a TEV-200 voltage clamp amplifier (Dagan Corp., Minneapolis, MN) and a DigiData 1440A interface (Molecular Devices). Data acquisition and analyses were done with pCLAMP 8 or 9 (Molecular Devices). Oocytes were placed in a recording chamber from Warner Instruments (Hamden, CT) and perfused with bath solutions at a constant flow rate of 12–15 ml/min. Oocytes were continuously clamped at −60 or −100 mV as specified in the figure legends.

Na^+ Self-inhibition Response—Na^+ self-inhibition responses were examined as described previously (36, 37). Briefly, Na^+ self-inhibition was determined by measuring the decrease in current from the peak (I_{peak}) to a steady state (I_{ss}) elicited by a rapid increase in extracellular Na^+ concentration from 1 to 110 mM. The $[Na^+]$ jump was done by rapidly replacing a 1 mM Na^+ bath solution (NaCl-1 containing 1 mM NaCl, 109 mM *N*-methyl-D-glucamine, 2 mM KCl, 2 mM $CaCl_2$, and 10 mM HEPES, pH 7.4) with a 110 mM Na^+ bath solution (NaCl-110 containing 110 mM NaCl, 2 mM KCl, 2 mM $CaCl_2$, and 10 mM HEPES, pH 7.4). Rapid solution exchange was performed with a 16-channel Teflon valve perfusion system (AutoMate Scientific, Inc., Berkeley, CA). The magnitude of Na^+ self-inhibition was represented by the ratio of amiloride-sensitive I_{ss} and I_{peak}.

Zn^{2+} Dose Responses—A 1 M $ZnCl_2$ stock solution (super pure, >99.999%, Sigma-Aldrich) was prepared in water and diluted to the desired concentrations in NaCl-110 bath solution. To examine Zn^{2+} dose responses, oocytes expressing mENaCs were continuously clamped at −60 mV while Zn^{2+} was applied at increasing concentrations in the range of 0.1 μM to 5 mM. Due to the limited solubility of $ZnCl_2$ in NaCl-110 bath solution, Zn^{2+} concentrations >5 mM were not tested. At the end of an experiment, 10 μM amiloride was added to the bath to determine the amiloride-sensitive current. The changes in amiloride-sensitive currents in response to Zn^{2+} applications were used to analyze the dose-response relationship.

Because the amiloride-sensitive current demonstrated a biphasic dose-response relationship with $[Zn^{2+}]$, we assumed that ENaCs possess a high-affinity activating site and a low-affinity inhibitory site for Zn^{2+}. Thus, the normalized currents in the presence of increasing concentrations of Zn^{2+} were fitted with Equation 1,

$$I_R = (I_{max} - I_{min})(C/(C + EC_{50}))(IC_{50}/(C + IC_{50})) + I_{min} \quad \text{(Eq. 1)}$$

where I_R is the relative current at certain $[Zn^{2+}]$ (*i.e.* current in the presence of Zn^{2+} normalized to current in the absence of Zn^{2+}); I_{max} and I_{min} are the maximal and minimal normalized currents, respectively; C is the Zn^{2+} concentration; and EC_{50} and IC_{50} are the concentrations with 50% effects for the activating and inhibitory phases, respectively.

Statistical Analysis—Data are presented as means ± S.E. To minimize bias from batch-to-batch variation in oocytes, the significance in the differences between mutant and WT channels was always analyzed from data obtained in the same batches of oocytes. Student's *t* tests were used for comparison, and the significance levels are specified below and in the figure legends. Curve fittings were performed with OriginPro 8.5 (OriginLab, Northampton, MA).

RESULTS

External Zn^{2+} Regulates mENaC by Interacting at Distinct Sites—Because extracellular Zn^{2+} activates ENaC by relieving Na^+ self-inhibition (25), the Na^+ self-inhibition response and the effect of Zn^{2+} were examined sequentially in each oocyte.

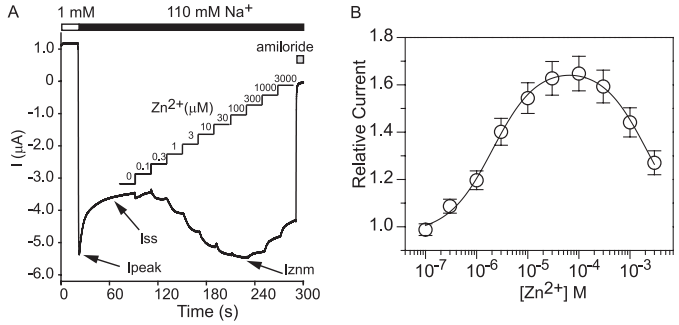

FIGURE 1. **External Zn^{2+} activates $\alpha\beta\gamma$mENaC with a bell-shaped dose-response.** *A*, a representative trace for Na^+ self-inhibition response and the effect of Zn^{2+} on mENaC. The peak current (I_{peak}), steady-state current (I_{ss}), and the maximal current in the presence of Zn^{2+} (I_{znm}) are indicated by *arrows*. *White*, *black*, and *gray bars* indicate the time periods when oocytes were bathed in low Na^+ (NaCl-1), high Na^+ (NaCl-110), and 10 μM amiloride solutions, respectively. The concentrations of Zn^{2+} in NaCl-110 bath solution are shown by *stepped lines* and *numbers* above. This recording represents 39 independent observations in six batches of oocytes. *B*, dose response of WT mENaC to Zn^{2+}. Relative currents are ratios of amiloride-sensitive currents obtained in the presence of Zn^{2+} and the currents measured immediately prior to Zn^{2+} application. The *line* is from a best fit of the data with the two-site model described under "Experimental Procedures" ($R^2 = 0.995$). The parameters were as follows: $I_{max} = 1.68$; $EC_{50} = 2.1$ μM; $IC_{50} = 2.1$ mM; and $I_{min} = 0.97$. The averaged data are from six observations in one batch of oocytes, representative of six independent experiments performed in different batches of oocytes.

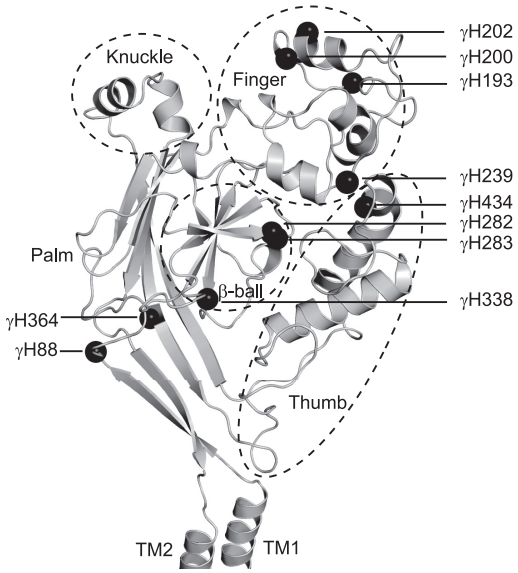

FIGURE 2. **Mapping the extracellular His residues of γmENaC on the cASIC1 structure.** A structural model for the ECD of one ASIC1 subunit was generated from ordinates in the Protein Data Bank (code 3HGC) using PyMOL 1.3 (50). Secondary structures in the model are shown as *gray ribbons* and *lines*. *Dashed lines* encircle four of the five subdomains within the ECD, and the left-out region belongs to the palm subdomain. Extracellular ends of the two transmembrane domains (*TM1* and *TM2*) are shown to reveal the covalent connections between the transmembrane domains and ECD. The *black spheres* show the locations of α-carbons of ASIC1 residues that are homologous to the His residues of γmENaC, based on sequence alignments. The locations of the four finger subdomain γHis residues are less certain than those of other residues, given the poor homology of this region among ENaC/degenerin family members. They serve as possible locations from one particular sequence alignment.

The Na^+ self-inhibition response reflects a decrease in current from a peak (I_{peak}) to a steady state (I_{ss}), which is elicited by a rapid increase in the extracellular Na^+ concentration from 1 to 110 mM (Fig. 1). As currents approached a steady-state level, increasing concentrations of Zn^{2+} were applied, and changes in current were measured. Increasing extracellular [Zn^{2+}] in the range of ~0.1–100 μM led to a dose-dependent increase in current. The current fell when extracellular [Zn^{2+}] was increased above 100 μM. The maximal current in the presence of Zn^{2+} (I_{znm}) was essentially identical to the I_{peak} observed following the increase in extracellular [Na^+] ($I_{znm}/I_{peak} = 1.00 \pm 0.01$, $n = 32$), consistent with the notion that Zn^{2+} relieves ENaC from inhibition by external Na^+.

Fig. 1*B* illustrates the Zn^{2+} dose-response relationship. Mean amiloride-sensitive currents in the presence of increasing extracellular [Zn^{2+}] were normalized to the base-line current. Similar to our previous report (25), we observed a bell-shaped dose response to Zn^{2+}. This relationship fits a model of ENaC possessing a high-affinity Zn^{2+} activating site and a low-affinity Zn^{2+} inhibitory site ($R^2 = 0.997$, Equation 1, see "Experimental Procedures") with an estimated EC_{50} and IC_{50} of 2.1 $\pm$ 0.1 μM ($n = 6$) and 2.1 $\pm$ 0.1 mM ($n = 6$), respectively. The maximal relative current observed at 100 μM Zn^{2+} was 1.68 $\pm$ 0.07 ($n = 6$).

Ala Substitutions of Selected His Residues in the Extracellular Region of γmENaC Alter the Effect of Zn^{2+}—There are a total of 10 His residues within the ECD of the γ-subunit. Four residues are located within the finger subdomain, three in the β-ball subdomain, two in the palm subdomain, and one in the thumb subdomain (Fig. 2). We individually mutated these His residues to Ala and expressed the mutant γ-subunits together with WT α- and β-subunits in oocytes. We sequentially examined Na^+ self-inhibition and the response to Zn^{2+} (Figs. 3 and 4) to determine whether a mutation selectively disrupted the effect of Zn^{2+} on channel activity or secondarily altered the Zn^{2+} effect by modifying the Na^+ self-inhibition response.

Ala substitutions at 4 of the 10 extracellular γ-subunit His residues (γH193A, γH200A, γH202A, and γH239A) significantly reduced maximal ENaC activation by Zn^{2+} (Figs. 3 and 4). Interestingly, all four of the extracellular His residues whose mutations reduced Zn^{2+} activation are within the predicted finger subdomain of the channel. In addition to suppressing Zn^{2+} activation, γH239A also diminished Na^+ self-inhibition, similar to what was previously observed when γHis^{239} was substituted with other residues (37, 38). As the γH239A mutant was relieved of Na^+ self-inhibition prior to the addition of Zn^{2+}, it is not possible to determine whether this residue is involved in Zn^{2+} binding to the channel. On the other hand, γH193A, γH200A, and γH202A did not significantly alter the Na^+ self-inhibition response, suggesting that these three His residues in the finger subdomain have specific roles in Zn^{2+} activation of ENaC.

Although γH88A did not affect the maximal Zn^{2+} activation ($p > 0.05$ *versus* WT) or the Na^+ self-inhibition response, it converted the Zn^{2+} dose response from bell-shaped to monophasic by selectively eliminating the inhibitory effect of high [Zn^{2+}] (Figs. 3 and 4). These results are consistent with a mutation-induced loss of a low-affinity Zn^{2+}-binding site that mediates channel inhibition at high [Zn^{2+}]. One mutation (γH283A) moderately increased the maximal Zn^{2+} activation ($p < 0.01$ *versus* WT) (Fig. 4). Collectively, these observations suggest that γHis^{88} within the palm subdomain and γHis^{193},

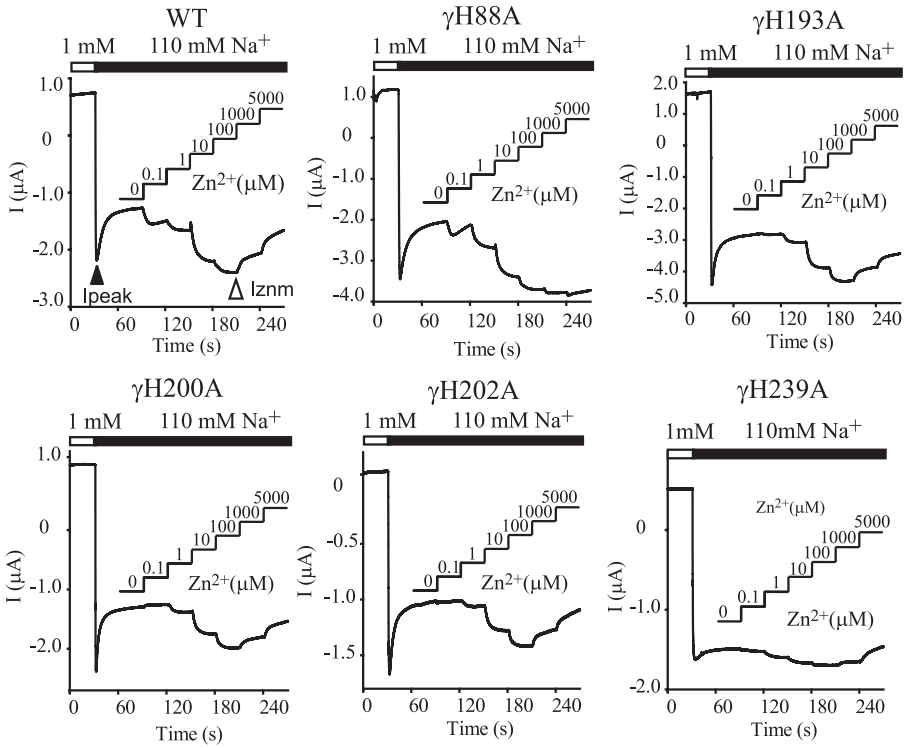

FIGURE 3. **Mutations of five γHis residues differentially alter the effect of Zn^{2+}.** Representative traces for current changes in responses to [Na^+] increases and Zn^{2+} applications are from oocytes expressing $\alpha\beta\gamma$mENaC (WT), $\alpha\beta\gamma$H88A, $\alpha\beta\gamma$H193A, $\alpha\beta\gamma$H200A, $\alpha\beta\gamma$H202A, and $\alpha\beta\gamma$H239A mENaCs. A simplified protocol for examining the effects of Zn^{2+} at only six concentrations compared with the one in Fig. 1 was used for both WT and mutant channels. The recording portions with 10 μM amiloride at the end of the experiments were omitted for clarity. These recordings represent at least six observations.

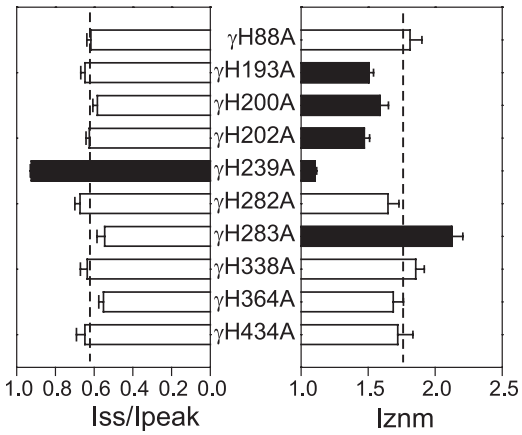

FIGURE 4. **Mutation-induced changes in the magnitude of Na^+ self-inhibition and the maximal Zn^{2+} activation of mENaC.** I_{ss}/I_{peak} values are inversely proportional to the magnitude of Na^+ self-inhibition. I_{znm} values represent the maximal relative currents in the presence of Zn^{2+}. They were typically observed with 100 μM Zn^{2+} except for the γH88A mutant, which had I_{znm} at 1 mM. Note that I_{znm} is the observed value and different from the I_{max} (Table 1) that was derived from a best fit of the dose-response data. *Black bars* indicate that the values of mutants were significantly different ($p < 0.01$) from those of WT (n = 5–10), obtained in the same batch of oocytes. The *dashed lines* show the mean values pooled from all oocytes expressing WT mENaC obtained in the analyses of these mutants (I_{ss}/I_{peak} = 0.60 ± 0.01, I_{znm} = 1.73 ± 0.03, n = 32).

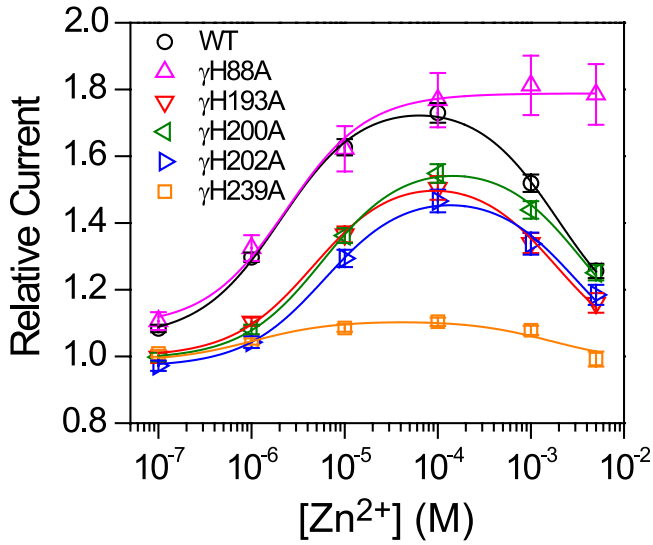

FIGURE 5. **Ala substitutions of five γHis residues result in distinct changes in the Zn^{2+} dose response.** Dose-response data are from the experiments performed as shown in Fig. 3 (n = 34 for WT and 6–15 for mutants). Curve fittings were done in the same way as described in the legend to Fig. 1. Parameters from the best fits of the averaged data were as follows: I_{max} = 1.77, EC_{50} = 2.1 μM, and IC_{50} = 1.9 mM for WT; I_{max} = 1.79, EC_{50} = 2.4 μM, and IC_{50} > 1 M for γH88A; I_{max} = 1.55, EC_{50} = 4.6 μM, and IC_{50} = 1.9 mM for γH193A; I_{max} = 1.59, EC_{50} = 5.9 μM, and IC_{50} = 3.6 mM for γH200A; I_{max} = 1.50, EC_{50} = 6.1 μM, and IC_{50} = 3.0 mM for γH202A; and I_{max} = 1.11, EC_{50} = 1.0 μM, and IC_{50} = 1.6 mM for γH239A. Fitting parameters from individual oocytes expressing WT and mutants (means ± S.E.) were compared for statistical differences (Table 1).

γHis^{200}, and γHis^{202} within the finger subdomain are involved in Zn^{2+}-dependent regulation of ENaC.

Mutation of γHis^{193}, γHis^{200}, or γHis^{202} within the Finger Subdomain Reduces the Apparent Zn^{2+} Binding Affinity of the Activating Site—We analyzed the responses of WT and mutant channels to increasing [Zn^{2+}] using a two-site model. Representative dose-response curves are shown in Fig. 5, and derived values for EC_{50} and IC_{50} are shown in Table 1. Our results show that γH88A did not affect the EC_{50} for the activating site,

although it essentially eliminated the decrease in channel activity observed with higher [Zn^{2+}]. In contrast, γH193A, γH200A, and γH202A reduced the sensitivity of mENaC to activation by extracellular Zn^{2+} and did not affect the inhibitory effect of high [Zn^{2+}], leading to increased EC_{50} values and no change in the IC_{50} relative to WT. The results imply that γH193A, γH200A, and γH202A selectively reduce the apparent affinity of the potentiating site for Zn^{2+} while not interfering with the low-affinity Zn^{2+} inhibitory site.

We also examined whether substitutions at multiple His residues led to further increases in the EC_{50} for Zn^{2+}. The Zn^{2+} dose-response relationships of γH200A/γH202A and γH193A/γH200A/γH202A were similar to those found in single mutants (Fig. 6). Thus, all three His residues within the finger subdomain are required for Zn^{2+}-dependent channel activation. The lack of an additive effect of multiple His substitutions suggests that these His residues participate in a common Zn^{2+}-binding site.

In addition to increasing the EC_{50} values of Zn^{2+} activation, γH193A, γH200A, γH202A, γH200A/γH202A, and γH193A/γH200A/γH202A also reduced the magnitude of the increase in current in response to Zn^{2+} (I_{max}) (Table 1). The reduced I_{max} observed in the mutants could be explained either by a reduction in the efficacy of channel activation by Zn^{2+} or by the presence of an inhibitory effect that limits the extent of channel activation. To distinguish these two possibilities, we examined channels with His substitutions at Zn^{2+} activating sites (γH200A/γH202A) and the Zn^{2+} inhibitory site (γH88A). As shown in Fig. 6*E*, γH88A/γH200A/γH202A reduced Zn^{2+} sensitivity by 8-fold compared with γH88A channels (EC_{50} = 20.4 ± 3.0 μM ($n = 6$) *versus* 2.6 ± 0.3 μM ($n = 10$); $p < 0.001$). However, both mutants had similar I_{max} values (1.81 ± 0.11 ($n = 6$) *versus* 1.79 ± 0.09 ($n = 10$); $p > 0.05$), demonstrating that mutations of the Zn^{2+} activating sites within the finger subdomain do not alter the magnitude of the maximal Zn^{2+} activation when the low-affinity Zn^{2+} inhibitory site is not

TABLE 1

Fitting parameters for Zn^{2+} dose responses

Parameters were from best fits of the dose-response data by nonlinear curve fitting, as described under "Experimental Procedures." Values are means ± S.E., averaged from individual oocytes expressing either WT or mutant channels. Parameters for WT channels were pooled from nine batches of oocytes that were used in the experiments and intended for reference. Student's *t* tests were done between the WT and mutant channels in the same batch of oocytes. All oocytes were injected with cRNAs for the WT mENaC α- and β-subunits together with either the WT or mutant mENaC γ-subunit.

	Oocytes	I_{max}	EC_{50}	IC_{50}
			μM	mM
WT	44	1.76 ± 0.03	2.10 ± 0.12	2.13 ± 0.14
γH88A	10	1.79 ± 0.09	2.58 ± 0.32	>1000
γH193A	6	1.54 ± 0.03[a]	4.59 ± 0.46[a]	1.97 ± 0.28
γH200A	14	1.59 ± 0.03[a]	5.94 ± 0.27[a]	3.69 ± 0.02
γH202A	15	1.50 ± 0.04[a]	6.29 ± 0.56[a]	3.22 ± 0.36
γH239A	9	1.18 ± 0.02[a]	3.03 ± 0.77	1.09 ± 0.24[a]
γH282A	10	1.69 ± 0.09	1.79 ± 0.31	1.61 ± 0.21
γH283A	5	2.20 ± 0.09[a]	2.11 ± 0.31	1.31 ± 0.10[a]
γH338A	5	1.88 ± 0.06	2.02 ± 0.37	3.10 ± 0.63
γH364A	6	1.74 ± 0.07	2.44 ± 0.25	1.68 ± 0.28
γH434A	12	1.61 ± 0.07	1.91 ± 0.24	1.71 ± 0.18
γH200A/γH202A	9	1.45 ± 0.03[a]	6.74 ± 0.52[a]	2.46 ± 0.36
γH193A/γH200A/γH202A	6	1.48 ± 0.03[a]	6.41 ± 0.48[a]	1.34 ± 0.23
γH88A/γH200A/γH202A	6	1.81 ± 0.11	20.4 ± 3.00[a]	>1000

[a] The values were significantly different from the WT values in the same batch of oocytes ($p < 0.01$).

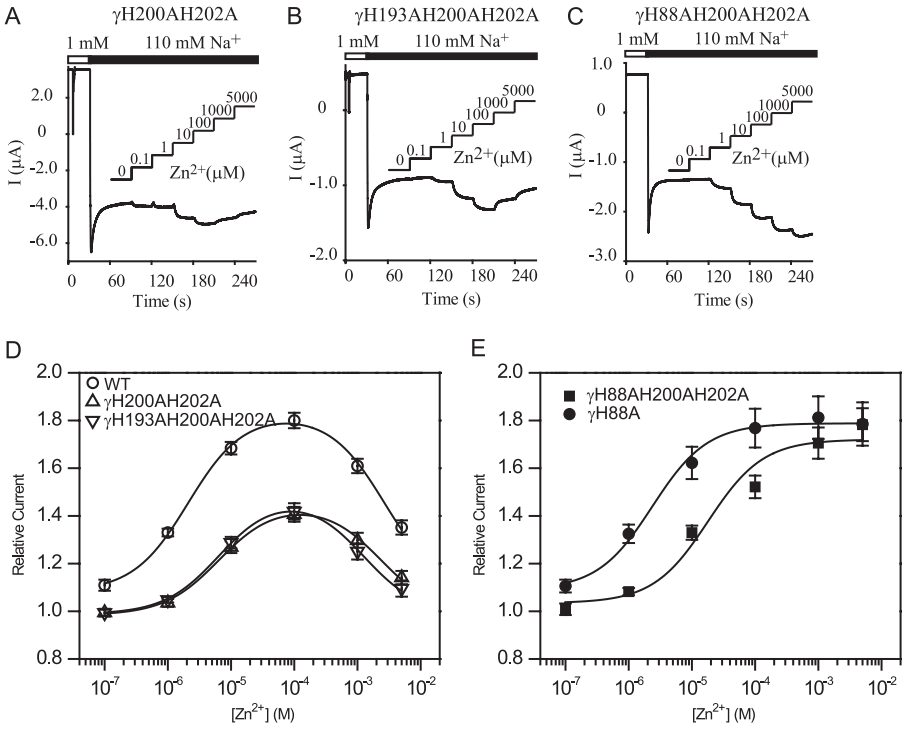

FIGURE 6. **Effects of Zn^{2+} on double and triple γHis mutations.** Representative traces are from oocytes expressing αβγH200A/γH202A (*A*; $n = 9$), αβγH193A/γH200A/γH202A (*B*; $n = 6$), and αβγH88A/γH200A/γH202A (*C*; $n = 6$) mENaCs. Experiments were performed as described in the legend to Fig. 3. Curve fittings in *D* and *E* were carried out as described in the legend to Fig. 5. Derived parameters in *D* were as follows: I_{max} = 1.82, EC_{50} = 2.1 μM, and IC_{50} = 2.7 mM for WT; I_{max} = 1.45, EC_{50} = 6.5 μM, and IC_{50} = 2.3 mM for γH200A/γH202A; and I_{max} = 1.48, EC_{50} = 6.5 μM, and IC_{50} = 1.2 mM for γH193A/γH200A/γH202A. Parameters in *E* were as follows: I_{max} = 1.79, EC_{50} = 2.4 μM, and IC_{50} > 1 M for γH88A and I_{max} = 1.72, EC_{50} = 18.0 μM, and IC_{50} > 1 M for γH88A/γH200A/γH202A. Parameters from individual oocytes are shown in Table 1.

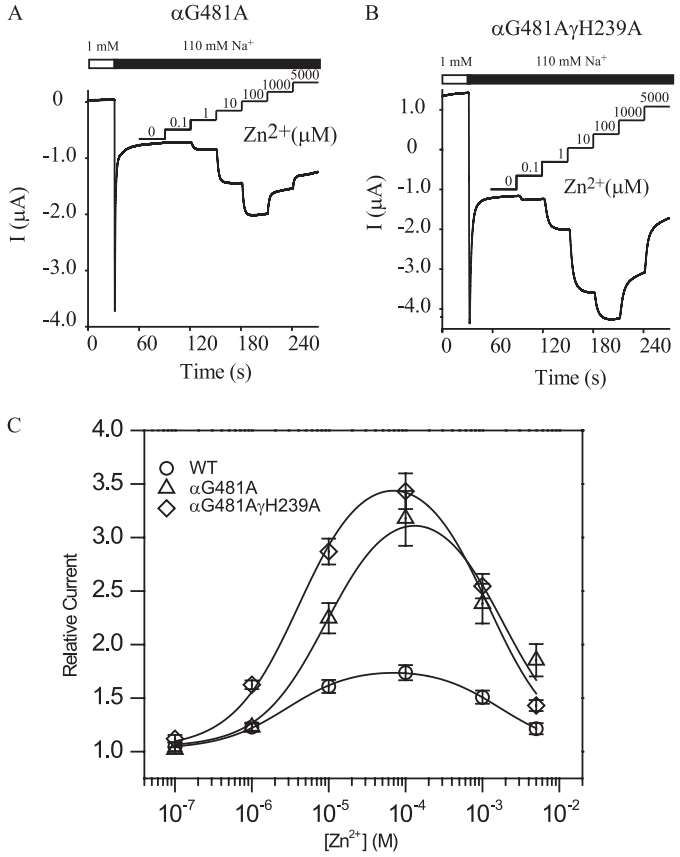

FIGURE 7. **Na^+ self-inhibition-enhancing mutation αG481A "restores" Zn^{2+} activation that is diminished by γH239A.** *A*, representative recording in oocytes expressing αG481Aβγ mENaC ($n = 6$). *B*, representative recording of αG481A/βγH239A mENaC ($n = 6$). *C*, dose-response curves. Fitting parameters were as follows: $I_{max} = 1.80$, $EC_{50} = 2.9$ μM, and $IC_{50} = 1.7$ mM for WT; $I_{max} = 3.4$, $EC_{50} = 9.6$ μM, and $IC_{50} = 1.8$ mM for αG481Aβγ; and $I_{max} = 3.7$, $EC_{50} = 4.2$ μM, and $IC_{50} = 1.2$ mM for αG481A/βγH239A.

present. Considered together, these results are consistent with the idea that γH200A/γH202A reduces the apparent Zn^{2+} binding affinity for the activating site without altering its efficacy. The inhibitory site containing γHis^{88} limits the efficacy of channel activation by Zn^{2+}.

γHis^{239} Does Not participate in Zn^{2+} Binding—The γH239A mutation eliminated both Na^+ self-inhibition and Zn^{2+} activation of ENaC (Figs. 3–5). As Zn^{2+} activates ENaC through relief of Na^+ self-inhibition, it is unclear whether γHis^{239} is a Zn^{2+}-binding site similar to the other finger subdomain His residues or whether the γH239A mutation simply prevents channel inhibition by external Na^+. To distinguish between these two possibilities, additional mutations were added to restore Na^+ self-inhibition in the setting of the γH239A mutant. Previously, we found that the G481A mutation within the α-subunit greatly enhanced the Na^+ self-inhibition response (39). Channels bearing both the αG481A and γH239A mutations exhibited a robust Na^+ self-inhibition response and a biphasic response to Zn^{2+} (Fig. 7). Both αG481A and αG481A/γH239A channels had I_{max} values that were significantly greater than the WT values (3.4 ± 0.2 ($n = 6$) and 3.7 ± 0.2 ($n = 6$), respectively), presumably as a result of the enhanced Na^+ self-inhibition. The EC_{50} for Zn^{2+} activation of αG481A/γH239A was similar to that of WT (4.2 ± 0.5 μM ($n = 6$) *versus* WT; $p > 0.05$), as was the IC_{50} of the Zn^{2+} inhibitory response (1.2 ± 0.0 mM ($n = 6$) *versus* WT; $p > 0.05$). Thus, γH239A did not weaken the apparent Zn^{2+} affinity of either the high- or low-affinity site.

Region Surrounding γHis^{88} Is a Determinant of the Low-affinity Inhibitory Site for Zn^{2+}—Next, the importance of the palm subdomain γHis^{88} and surrounding region was examined to explore the nature of the low-affinity Zn^{2+} inhibitory site. As shown in Figs. 3 and 5, mutation of γHis^{88} to Ala prevented ENaC inhibition by high concentrations of Zn^{2+}. Mutation of γHis^{88} to either Arg or Asp also rendered the Zn^{2+} dose responses monophasic and did not significantly alter the Na^+ self-inhibition response (Fig. 8, *A* and *B*). These results suggest that a His residue at this position is an essential determinant of the Zn^{2+} inhibitory site.

Zn^{2+} is often coordinated by multiple neighboring amino acid residues in metal-binding proteins (32). To define additional residues that contribute to the low-affinity Zn^{2+} inhibitory site, we searched for additional potential Zn^{2+}-binding residues using sequence alignments of ENaC and ASIC and the resolved cASIC1 structure (40). γHis^{88} aligns with Ala^{82} in cASIC1, which is located immediately after the first β-strand of ECD (β1) within the palm subdomain (Fig. 8*C*). Multiple regions within the same subunit (strand β1 and loops β1-β2, β11-β12, and β5-β6) and an adjacent subunit (N-terminal end of helix α4 and loop α5-β10) are in close proximity to Ala^{82} in cASIC1. Eleven residues in these regions are within 6 Å of the Ala^{82} (Fig. 8*C*). Among these residues, only Ala^{413} and Met^{364} have homologous residues in mENaC that are often found within a Zn^{2+} coordination shell (γAsp^{516} and βGlu^{444}, respectively). We examined whether these sites are involved in ENaC regulation by Zn^{2+}. As shown in Fig. 8 (*D* and *E*), γD516A and γD516R largely prevented ENaC inhibition by high $[Zn^{2+}]$, similar to what we observed with the γH88A mutant (Fig. 5). Mutation of the other residue that was predicted to be in close proximity to γHis^{88} (βE444A) did not significantly alter the Zn^{2+} effects on ENaC (data not shown). The proximity of γAsp^{516} to γHis^{88} and their similar mutation-induced changes in the Zn^{2+} response suggest that the two residues share a functional role in constituting the low-affinity Zn^{2+} inhibitory site.

The residues corresponding to γHis^{88} and γAsp^{516} in cASIC1 (Ala^{82} and Ala^{413}) are located at a subunit interface (Fig. 8*C*). According to the suggested counterclockwise arrangement (viewed from above) of the ENaC α-, β-, and γ-subunits (14, 28), γHis^{88} (Ala^{82} in cASIC1) and γAsp^{516} (Ala^{413} in cASIC1) are expected to interact with residues within the thumb subdomain of βENaC. There are five negatively charged βENaC residues within loops β9-α4 and α5-β10 of the thumb subdomain: βGlu^{354}, βAsp^{365}, βGlu^{436}, βGlu^{444}, and βGlu^{448}. Given their locations within flexible loops, they might be in close proximity to γHis^{88} and γAsp^{516} and contribute to the low-affinity inhibitory site. Mutations of these β-subunit residues to Ala did not alter the channel's response to Zn^{2+} (data not shown). Thus, it is unlikely that these residues within the thumb domain of βENaC are involved in Zn^{2+} regulation of the channel.

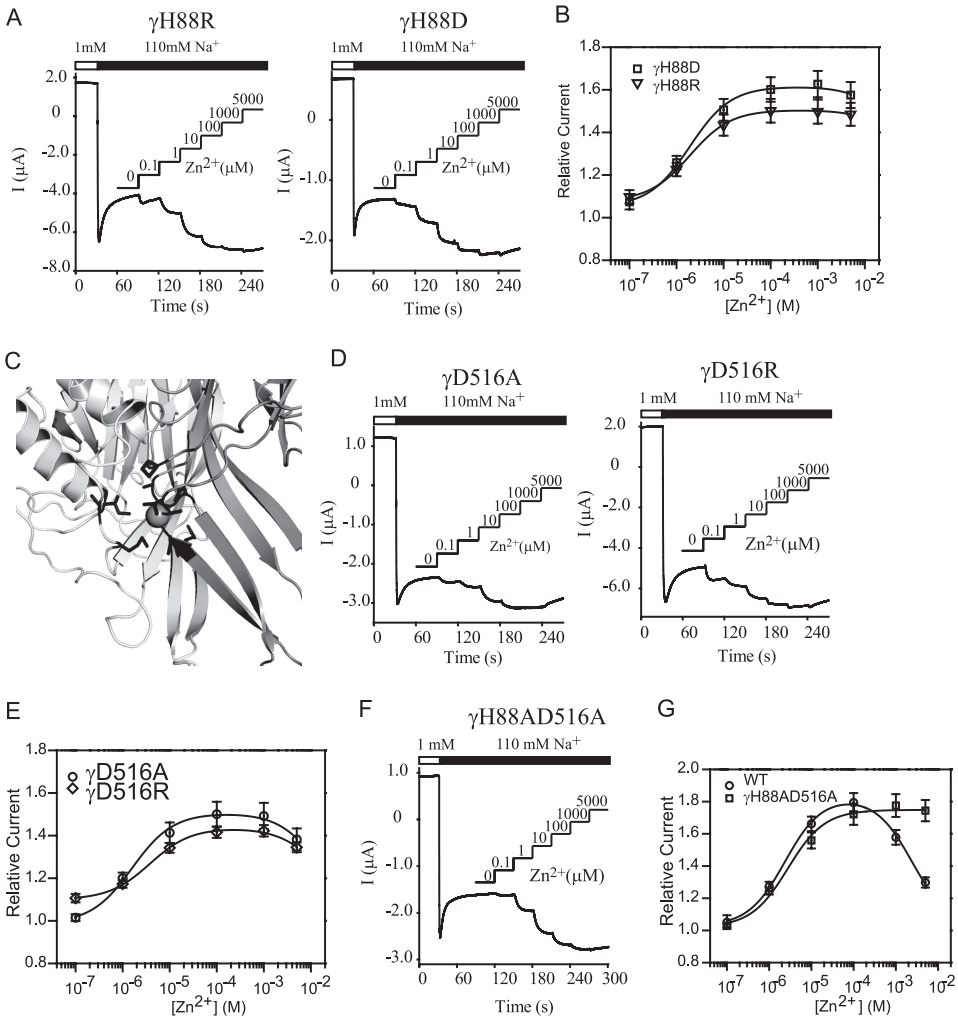

FIGURE 8. **Mutations of γHis^{88} and γAsp^{516} eliminate the inhibitory component in the Zn^{2+} dose response.** *A*, traces for γH88R and γH88D. *B*, dose-response curves of γHis^{88} mutants. Fitting parameters were as follows: I_{max} = 1.62, EC_{50} = 1.9 μM, and IC_{50} = 72.8 mM for αβγH88D and I_{max} = 1.52, EC_{50} = 1.9 μM, and IC_{50} = 96.3 mM for αβγH88R. *C*, a model of cASIC1 was generated from coordinates in the Protein Data Bank (code 3HGC) using PyMOL 1.3 (50) to show the local structure within the ECD at the interface of subunits B (*dark gray*) and C (*light gray*). *Black* lines depict residues that are within 6 Å of Ala^{82}, shown as a *sphere*. *D*, representative traces of γD516A and γD516R. *E*, dose-response curves of γD516A and γD516R. Fitting parameters were as follows: I_{max} = 1.51, EC_{50} = 1.6 μM, and IC_{50} = 16.6 mM for αβγD516A and I_{max} = 1.44, EC_{50} = 3.8 μM, and IC_{50} = 13.9 mM for αβγD516R. *F*, trace of αβγH88A/γD516A. *G*, dose responses for WT and αβγH88A/γD516A mENaCs. Fitting parameters were as follows: I_{max} = 1.83, EC_{50} = 2.4 μM, and IC_{50} = 2.4 mM for WT and I_{max} = 1.74, EC_{50} = 2.8 μM, and IC_{50} > 1 M for αβγH88A/γD516A.

DISCUSSION

The major goal of this study was to probe the structural basis of the regulation of ENaC by Zn^{2+}. The biphasic dose response of Zn^{2+} on the purinergic receptor P2X is believed to originate from Zn^{2+} binding at two distinct sites within the receptor: a high-affinity activating site and a low-affinity inhibitory site (41). Because the ENaC/degenerin family is structurally similar to P2X (40), we hypothesized that the bell-shaped Zn^{2+} dose-response relationship with ENaC activity is due to the presence of a high-affinity activating site and a low-affinity inhibitory site within the ECD. We found that a minimal two-site model sufficiently describes the bell-shaped dose response of mouse ENaC to external Zn^{2+}. The presence of a high-affinity activating site and a low-affinity inhibitory site is supported by our observations that Zn^{2+}-mediated activation or inhibition can be selectively eliminated by targeted mutations of specific residues in the activating site or the inhibitory site, respectively. On the basis of these observations, we propose that γHis^{193}, γHis^{200}, and γHis^{202} within the finger subdomain contribute to a high-affinity Zn^{2+}-binding site and that γHis^{88} and γAsp^{516} in the palm subdomain are key determinants of a low-affinity Zn^{2+}-binding site (Fig. 9).

The following observations suggest that γHis^{193}, γHis^{200}, and γHis^{202}, presumably within the finger subdomain, contribute to a high-affinity Zn^{2+} activating site. (i) Mutation of these residues increased the EC_{50} of Zn^{2+} activation and had no effect on the IC_{50} (Fig. 5 and Table 1), suggesting that these residues are specifically involved in Zn^{2+} binding to an activating site. (ii) Although mutations of γHis^{193}, γHis^{200}, and γHis^{202} reduced the maximal ENaC current elicited by Zn^{2+}, maximal Zn^{2+} activation was not affected when the Zn^{2+} inhibitory site was also mutated (γH88A/γH200A/γH202A). Thus, γH200A/γH202A appears to primarily affect the apparent affinity of the activating site and does not alter the efficacy of channel activation. (iii) γHis^{193}, γHis^{200}, and γHis^{202} appear to share a similar functional role in mediating Zn^{2+} effects on

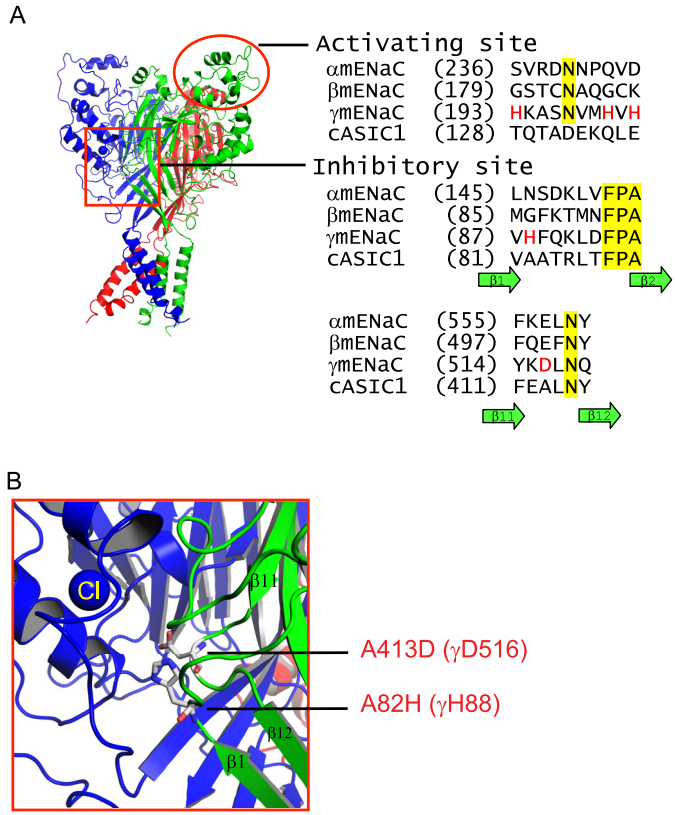

FIGURE 9. **Finger and palm subdomains of γENaC contain key sites for Zn^{2+} interaction with the channel.** *A*, a structural model of cASIC1. Three ASIC1 subunits are rendered as *colored ribbons* from coordinates in the Protein Data Bank (code 3HGC) (40). The *red circle* identifies the finger subdomain of ASIC1 to show the likely locations of γHis[193], γHis[200], and γHis[202] that are proposed to contribute to the high-affinity activating Zn^{2+}-binding site. Their exact homologous sites within the ASIC1 structure are not known due to a low level of sequence homology in the finger subdomains. The sequence alignments of mouse, rat, and human α-, β-, and γ-subunits and cASIC1 were performed with Vector NTI 11.0 (Invitrogen). Rat and human ENaC sequences are omitted for clarity. The three His residues are shown in *red*. The *red square* shows a subunit interface between the palm subdomain of the *green* subunit and the thumb subdomain of the *blue* subunit, where γHis[88] and γAsp[516] are proposed to reside in a mENaC structure and contribute to the low-affinity inhibitory Zn^{2+}-binding site. The *green* ASIC1 subunit was arbitrarily considered to correspond to γmENaC. The sequences of loops β1-β2 and β11-β12 of αβγmENaC and cASIC1 are shown with identical residues highlighted in *yellow* and γHis[88] and γAsp[516] in *red*. *B*, enlargement of the area enclosed by the *red square* in *A*. Three β-strands (β1, β11, and β12) are labeled as in the literature (40). The γHis[88]-homologous Ala[82] and γAsp[516]-homologous Ala[413] residues were mutated to His and Asp, respectively, in the ASIC1 model. The *labeled blue sphere* shows Cl^- bound within the thumb subdomain of the *blue* subunit. Structural models were drawn using PyMOL 1.3 (50).

the channel. Individual mutation of any of the three His residues induced a similar phenotype, including an increase in EC_{50}, a decrease in maximal Zn^{2+} activation, and a lack of effect on Na^+ self-inhibition. Moreover, mutation-induced changes in EC_{50} were not additive in γH193A/γH200A/γH202A channels (Fig. 6*D*). (iv) Their proximity in the sequence makes it structurally possible for them to contribute to a common binding site. Interestingly, the His[200]-Val[201]-His[202] sequence matches a common Zn^{2+}-binding motif, HXH, where *X* can be any residue (42). This motif is also present in other channels (43, 44).

Channels with substitutions of all three His residues are still activated by Zn^{2+}, suggesting that there are additional sites within the channel where Zn^{2+} binds and activates ENaC. It is notable that His residues are not present at sites in the α- and β-subunits that correspond to γHis[193], γHis[200], and γHis[202] (Fig. 9). Further studies are needed to identify additional sites involved in Zn^{2+} activation of ENaC.

Our results demonstrate that γHis[88] within the palm subdomain is a key determinant for the low-affinity inhibitory Zn^{2+}-binding site. Interestingly, like the three finger subdomain His residues, γHis[88] is also not conserved among ENaC subunits (Fig. 9). Taking advantage of the structural information of ASIC1, a negatively charged residue, γAsp[516], was identified that lies in close proximity to γHis[88] and is likely involved in the inhibitory effect of Zn^{2+} as well (Fig. 9). However, it is also possible that mutations of γHis[88] and γAsp[516] may diminish the inhibitory component in the biphasic Zn^{2+} dose response by disrupting conformational changes induced by Zn^{2+} binding, instead of abolishing Zn^{2+} binding. Nevertheless, our observations suggest that this region (loops β1-β2 and β11-β12), located at the middle of the palm subdomain, contributes to a general inhibitory site for different channel regulators (Fig. 9). Indeed, a putative Cl^--binding site and a Cu^{2+}-binding site have been identified near this region in human ENaCs (14, 28). The corresponding region in ASIC1 has been implicated in H^+ sensing and desensitization (27, 45–47). This solvent-accessible region appears to be an excellent target for the development of therapeutic agents that modulate activities of these related channels.

The activating effect of Zn^{2+} on ENaC depends on the presence of Na^+ self-inhibition (Figs. 3–5) (25). External Zn^{2+} may disrupt either Na^+ binding to its receptor site or Na^+-induced conformational changes. Our observations that mutations at the implicated Zn^{2+}-binding sites (γH193A, γH200A, γH202A, and γH88A) did not alter the Na^+ self-inhibition response suggest that the binding sites for Zn^{2+} and Na^+ are distinct. The lack of effect on the apparent affinity for Zn^{2+} activation of a mutation of a critical site for Na^+ self-inhibition (γH239A) also supports the notion of distinct Zn^{2+}- and Na^+-binding sites. Therefore, it is likely that Zn^{2+} binding interferes with Na^+-induced motions within the ECD. Similar to Zn^{2+}, several extracellular factors such as proteases, Cl^-, H^+, and small molecules are thought to regulate ENaC gating in part by altering the Na^+ self-inhibition response (13, 15, 28, 36, 48). It would be of great interest to determine whether other extracellular regulators affect Na^+ self-inhibition in a similar manner to Zn^{2+}.

Recent studies suggest that ENaCs may belong to ligand-gated channels, like other members of the ENaC/degenerin family (25, 26, 49). Multiple external regulators of ENaC, including transition metals, Cl^-, H^+, and other small molecules, exert their effects on ENaC gating by binding to regions within the ECD that are structurally distant from the channel pore (13–15, 28). These gating regulators are expected to remotely influence the channel gate through a series of conformational changes. The identification of these allosteric regulatory sites will advance our understanding regarding mechanisms by which the binding of allosteric regulators alters channel gating.

In summary, this study provides novel insights into the structural basis for Zn^{2+} regulation of ENaC. Our results suggest that external Zn^{2+} regulates ENaC activity by binding to mul-

tiple extracellular sites, including a high-affinity activating site in the finger subdomain and a low-affinity inhibitory site in the palm subdomain of the γ-subunit. These findings advance our understanding of the regulation of ENaC gating by extracellular factors.

Acknowledgments—We thank Dr. Thomas R. Kleyman for helpful discussions and Brandon M. Blobner for oocyte preparation.

REFERENCES

1. Rossier, B. C., Pradervand, S., Schild, L., and Hummler, E. (2002) Epithelial sodium channel and the control of sodium balance: interaction between genetic and environmental factors. *Annu. Rev. Physiol.* **64,** 877–897
2. Snyder, P. M. (2002) The epithelial Na^+ channel: cell surface insertion and retrieval in Na^+ homeostasis and hypertension. *Endocr. Rev.* **23,** 258–275
3. Bhalla, V., and Hallows, K. R. (2008) Mechanisms of ENaC regulation and clinical implications. *J. Am. Soc. Nephrol.* **19,** 1845–1854
4. Qadri, Y. J., Rooj, A. K., and Fuller, C. M. (2012) ENaCs and ASICs as therapeutic targets. *Am. J. Physiol. Cell Physiol.* **302,** C943–C965
5. Pratt, J. H. (2005) Central role for ENaC in development of hypertension. *J. Am. Soc. Nephrol.* **16,** 3154–3159
6. Soundararajan, R., Pearce, D., Hughey, R. P., and Kleyman, T. R. (2010) Role of epithelial sodium channels and their regulators in hypertension. *J. Biol. Chem.* **285,** 30363–30369
7. Büsst, C. J., Bloomer, L. D., Scurrah, K. J., Ellis, J. A., Barnes, T. A., Charchar, F. J., Braund, P., Hopkins, P. N., Samani, N. J., Hunt, S. C., Tomaszewski, M., and Harrap, S. B. (2011) The epithelial sodium channel γ-subunit gene and blood pressure: family-based association, renal gene expression, and physiological analyses. *Hypertension* **58,** 1073–1078
8. Van Driessche, W., and Zeiske, W. (1985) Ionic channels in epithelial cell membranes. *Physiol. Rev.* **65,** 833–903
9. Sheng, S., Johnson, J. P., and Kleyman, T. R. (2007) in *Seldin and Giebisch's The Kidney: Physiology & Pathophysiology* (Alpern, R. J., and Hebert, S. C. eds)pp. 743–768, 4th Ed., Academic Press, New York
10. Yu, L., Eaton, D. C., and Helms, M. N. (2007) Effect of divalent heavy metals on epithelial Na^+ channels in A6 cells. *Am. J. Physiol. Renal Physiol.* **293,** F236–D244
11. Kleyman, T. R., Carattino, M. D., and Hughey, R. P. (2009) ENaC at the cutting edge: regulation of epithelial sodium channels by proteases. *J. Biol. Chem.* **284,** 20447–20451
12. Collier, D. M., and Snyder, P. M. (2009) Extracellular protons regulate human ENaC by modulating Na^+ self-inhibition. *J. Biol. Chem.* **284,** 792–798
13. Collier, D. M., and Snyder, P. M. (2009) Extracellular chloride regulates the epithelial sodium channel. *J. Biol. Chem.* **284,** 29320–29325
14. Chen, J., Myerburg, M. M., Passero, C. J., Winarski, K. L., and Sheng, S. (2011) External Cu^{2+} inhibits human epithelial Na^+ channels by binding at a subunit interface of extracellular domains. *J. Biol. Chem.* **286,** 27436–27446
15. Molina, R., Han, D. Y., Su, X. F., Zhao, R. Z., Zhao, M., Sharp, G. M., Chang, Y., and Ji, H. L. (2011) Cpt-cAMP activates human epithelial sodium channels via relieving self-inhibition. *Biochim. Biophys. Acta* **1808,** 1818–1826
16. Mathie, A., Sutton, G. L., Clarke, C. E., and Veale, E. L. (2006) Zinc and copper: pharmacological probes and endogenous modulators of neuronal excitability. *Pharmacol. Ther.* **111,** 567–583
17. St Croix, C. M., Leelavaninchkul, K., Watkins, S. C., Kagan, V. E., and Pitt, B. R. (2005) Nitric oxide and zinc homeostasis in acute lung injury. *Proc. Am. Thorac. Soc.* **2,** 236–242
18. Adamson, I. Y., Prieditis, H., and Vincent, R. (1999) Pulmonary toxicity of an atmospheric particulate sample is due to the soluble fraction. *Toxicol. Appl. Pharmacol.* **157,** 43–50
19. Prieditis, H., and Adamson, I. Y. (2002) Comparative pulmonary toxicity of various soluble metals found in urban particulate dusts. *Exp. Lung Res.* **28,** 563–576
20. Restrepo-Angulo, I., De Vizcaya-Ruiz, A., and Camacho, J. (2010) Ion channels in toxicology. *J. Appl. Toxicol.* **30,** 497–512
21. Andreini, C., Banci, L., Bertini, I., and Rosato, A. (2006) Counting the zinc proteins encoded in the human genome. *J. Proteome Res.* **5,** 196–201
22. Chasapis, C. T., Loutsidou, A. C., Spiliopoulou, C. A., and Stefanidou, M. E. (2012) Zinc and human health: an update. *Arch. Toxicol.* **86,** 521–534
23. Harrison, N. L., and Gibbons, S. J. (1994) Zn^{2+}: an endogenous modulator of ligand- and voltage-gated ion channels. *Neuropharmacology* **33,** 935–952
24. Frederickson, C. J., Koh, J. Y., and Bush, A. I. (2005) The neurobiology of zinc in health and disease. *Nat. Rev. Neurosci.* **6,** 449–462
25. Sheng, S., Perry, C. J., and Kleyman, T. R. (2004) Extracellular Zn^{2+} activates epithelial Na^+ channels by eliminating Na^+ self-inhibition. *J. Biol. Chem.* **279,** 31687–31696
26. Kashlan, O. B., and Kleyman, T. R. (2011) ENaC structure and function in the wake of a resolved structure of a family member. *Am. J. Physiol. Renal Physiol.* **301,** F684–F696
27. Jasti, J., Furukawa, H., Gonzales, E. B., and Gouaux, E. (2007) Structure of acid-sensing ion channel 1 at 1.9 Å resolution and low pH. *Nature* **449,** 316–323
28. Collier, D. M., and Snyder, P. M. (2011) Identification of epithelial Na^+ channel (ENaC) intersubunit Cl^- inhibitory residues suggests a trimeric αγβ channel architecture. *J. Biol. Chem.* **286,** 6027–6032
29. Shi, S., Ghosh, D. D., Okumura, S., Carattino, M. D., Kashlan, O. B., Sheng, S., and Kleyman, T. R. (2011) Base of the thumb domain modulates epithelial sodium channel gating. *J. Biol. Chem.* **286,** 14753–14761
30. Kashlan, O. B., Adelman, J. L., Okumura, S., Blobner, B. M., Zuzek, Z., Hughey, R. P., Kleyman, T. R., and Grabe, M. (2011) Constraint-based homology model of the extracellular domain of the epithelial Na^+ channel α-subunit reveals a mechanism of channel activation by proteases. *J. Biol. Chem.* **286,** 649–660
31. Stewart, A. P., Haerteis, S., Diakov, A., Korbmacher, C., and Edwardson, J. M. (2011) Atomic force microscopy reveals the architecture of the epithelial sodium channel (ENaC). *J. Biol. Chem.* **286,** 31944–31952
32. Dokmanić, I., Sikić, M., and Tomić, S. (2008) Metals in proteins: correlation between the metal-ion type, coordination number, and the amino acid residues involved in the coordination. *Acta Crystallogr. D Biol. Crystallogr.* **64,** 257–263
33. Carattino, M. D., Hughey, R. P., and Kleyman, T. R. (2008) Proteolytic processing of the epithelial sodium channel γ-subunit has a dominant role in channel activation. *J. Biol. Chem.* **283,** 25290–25295
34. Diakov, A., Bera, K., Mokrushina, M., Krueger, B., and Korbmacher, C. (2008) Cleavage in the γ-subunit of the epithelial sodium channel (ENaC) plays an important role in the proteolytic activation of near-silent channels. *J. Physiol.* **586,** 4587–4608
35. Sheng, S., Perry, C. J., and Kleyman, T. R. (2002) External nickel inhibits epithelial sodium channel by binding to histidine residues within the extracellular domains of α- and γ-subunits and reducing channel open probability. *J. Biol. Chem.* **277,** 50098–50111
36. Chraïbi, A., and Horisberger, J. D. (2002) Sodium self inhibition of human epithelial sodium channel: temperature dependence and effect of extracellular proteases. *J. Gen. Physiol.* **120,** 133–145
37. Sheng, S., Bruns, J. B., and Kleyman, T. R. (2004) Extracellular histidine residues crucial for Na^+ self-inhibition of epithelial Na^+ channels. *J. Biol. Chem.* **279,** 9743–9749
38. Winarski, K. L., Sheng, N., Chen, J., Kleyman, T. R., and Sheng, S. (2010) Extracellular allosteric regulatory subdomain within the γ-subunit of the epithelial Na^+ channel. *J. Biol. Chem.* **285,** 26088–26096
39. Maarouf, A. B., Sheng, N., Chen, J., Winarski, K. L., Okumura, S., Carattino, M. D., Boyd, C. R., Kleyman, T. R., and Sheng, S. (2009) Novel determinants of epithelial sodium channel gating within extracellular thumb domains. *J. Biol. Chem.* **284,** 7756–7765
40. Gonzales, E. B., Kawate, T., and Gouaux, E. (2009) Pore architecture and ion sites in acid-sensing ion channels and P2X receptors. *Nature* **460,** 599–604
41. Coddou, C., Yan, Z., Obsil, T., Huidobro-Toro, J. P., and Stojilkovic, S. S.

(2011) Activation and regulation of purinergic P2X receptor channels. *Pharmacol. Rev.* **63,** 641–683
42. Karlin, S., and Zhu, Z. Y. (1997) Classification of mononuclear zinc metal sites in protein structures. *Proc. Natl. Acad. Sci. U.S.A.* **94,** 14231–14236
43. Choi, Y. B., and Lipton, S. A. (1999) Identification and mechanism of action of two histidine residues underlying high-affinity Zn^{2+} inhibition of the NMDA receptor. *Neuron* **23,** 171–180
44. Harvey, R. J., Thomas, P., James, C. H., Wilderspin, A., and Smart, T. G. (1999) Identification of an inhibitory Zn^{2+}-binding site on the human glycine receptor α_1-subunit. *J. Physiol.* **520,** 53–64
45. Li, T., Yang, Y., and Canessa, C. M. (2010) Asn^{415} in the β11-β12 linker decreases proton-dependent desensitization of ASIC1. *J. Biol. Chem.* **285,** 31285–31291
46. Li, T., Yang, Y., and Canessa, C. M. (2010) Leu^{85} in the β1-β2 linker of ASIC1 slows activation and decreases the apparent proton affinity by stabilizing a closed conformation. *J. Biol. Chem.* **285,** 22706–22712
47. Springauf, A., Bresenitz, P., and Gründer, S. (2011) The interaction between two extracellular linker regions controls sustained opening of acid-sensing ion channel 1. *J. Biol. Chem.* **286,** 24374–24384
48. Sheng, S., Carattino, M. D., Bruns, J. B., Hughey, R. P., and Kleyman, T. R. (2006) Furin cleavage activates the epithelial Na^+ channel by relieving Na^+ self-inhibition. *Am. J. Physiol. Renal Physiol.* **290,** F1488–F1496
49. Horisberger, J. D., and Chraïbi, A. (2004) Epithelial sodium channel: a ligand-gated channel? *Nephron. Physiol.* **96,** 37–41
50. DeLano, W. L. (2010) *The PyMOL Molecular Graphics System, Version 1.3*, Schrödinger, LLC, San Diego, CA